

1 Surprising simplicities and syntheses in limbless self-propulsion in sand  
2

3 Henry C. Astley, Joseph R. Mendelson III, Jin Dai, Chaohui Gong, Baxi Chong, Jennifer M.  
4 Rieser, Perrin Schiebel, Sarah S. Sharpe, Ross L. Hatton, Howie Choset, Daniel I. Goldman

5 Abstract

6 Animals moving on and in fluids and solids move their bodies in diverse ways to generate  
7 propulsion and lift forces. In fluids, animals can wiggle, stroke, paddle or slap, whereas on hard  
8 frictional terrain, animals largely engage their appendages with the substrate to avoid slip.  
9 Granular substrates, such as desert sand, can display complex responses to animal interactions.  
10 This complexity has led to locomotor strategies that make use of fluid-like or solid-like features  
11 of this substrate, or combinations of both. Here, we use examples from our work to demonstrate  
12 the diverse array of methods used and insights gained in the study of both surface and subsurface  
13 limbless locomotion in these habitats. We also provide insights into the origins of that most  
14 enigmatic of granular locomotor modes – sidewinding. Counterintuitively, these seemingly  
15 complex granular environments offer certain experimental, theoretical, robotic and  
16 computational advantages for studying terrestrial movement, with the potential for providing  
17 broad insights into morphology and locomotor control in fluids and solids, including  
18 neuromechanical control templates and morphological and behavioral evolution. In particular,  
19 granular media provide an excellent testbed for a locomotion framework called geometric  
20 mechanics, which was introduced by particle physicists and control engineers in the last century,  
21 and which allows quantitative analysis of alternative locomotor patterns and morphology to test  
22 for control templates, optimality and evolutionary alternatives. Thus, we posit that insights  
23 gained from movement in granular environments can be translated into principles that have  
24 broader applications across taxa, habitats and movement patterns, including those at microscopic  
25 scales.

26

27

28 Summary Statement: Dry sandy environments present challenges to animal locomotion, but are  
29 also amenable to several useful experimental and theoretical methods, which can generate  
30 uncommonly rich insights into animal locomotion.

31

32

33

34

35 **Introduction**

36 In recent years, the study of biomechanics has helped disentangle the roles of control and  
37 mechanics during locomotion in natural environments. During animal locomotion, coupled  
38 nervous, muscular and mechanical systems produce movements that generate reaction forces to  
39 move the body forward. Movement, however, cannot proceed without appropriate environmental  
40 interactions. Even common environments like hard ground, water and air display complex  
41 interactions with moving animals. For example, analysis of legged locomotion on flat rigid  
42 terrain can be complex due to impulsive and repeated collisions (e.g. (Collins et al., 2005;  
43 Holmes et al., 2006)). Fluid interactions have been extensively studied (Vogel, 1994; Lauder,  
44 2010), but despite possessing the partial differential equations that describe such interactions (the  
45 Navier–Stokes equations), the complexity of fluid flow around deforming bodies makes it  
46 difficult to gain a fundamental understanding of locomotion in these environments (Tobalske,  
47 2007; Tytell et al., 2010; Waldrop and Miller, 2015; Gemmell et al., 2016; Cohen et al., 2018;  
48 Wise et al., 2018).

49 *Granular media*

50 In environments composed of granular media (see Glossary) such as sand and loose soil,  
51 the situation is seemingly more complicated. Granular media comprise numerous discrete  
52 particles which, depending upon loading conditions, can jam together (see Glossary) via internal  
53 friction and behave as a solid, or they may slip past each other to yield and flow like a fluid  
54 (Gravish et al 2010). Granular media discussed here will be defined as collections of  
55 approximately spherical particles that interact via repulsive contact forces (friction and  
56 repulsion). Until recently, we have not had equations for granular materials that describe these  
57 fluid- and solid-like interactions under all conditions (see (Askari and Kamrin, 2016)); however,  
58 many insights have been gained through hundreds of years of study (Coulomb, 1776; Schofield  
59 and Wroth, 1968; Savage, 1984; (Andreotti et al., 2013). For example, provided that stresses do  
60 not exceed critical ‘yield’ stresses (see Glossary), granular media can support loads without  
61 significant deformation. However, if yield stresses are exceeded, the materials can enter a  
62 ‘frictional fluid’ state (see Glossary) that is peculiar compared to true fluids. For example, even  
63 at relatively large speeds of movement through granular media, reaction forces are insensitive to  
64 rate of movement (Geng and Behringer, 2005; [Maladen et al, 2009](#)), in contrast to the strong  
65 dependence upon velocity in fluids. This insensitivity is a consequence of the dominance and  
66 rate insensitivity of Coulomb friction (see Glossary) between particles and between particle and  
67 body elements (Maladen et al., 2009). Further, forces depend on compaction; a few percent in  
68 packing fraction (see Glossary) can lead to doubling of resistance forces.

69 Both solid- and fluid-like responses can be important to understand the control of  
70 locomotion on granular materials. For example, because the transitions between these two  
71 responses are sensitive to the kinematics of the intruding object, animals may modify their  
72 movements to promote solidification or fluidization of the media to improve their locomotor

73 performance (Mazouchova et al., 2010; Marvi et al., 2014). Further, the high frictional forces in  
74 sand and the ability of the material to ‘remember’ disturbances (e.g. footprints and tracks)  
75 impose additional demands on locomotion. These disturbed regions can have lower yield stress;  
76 thus, an animal that interacts with disturbed media may have reduced displacement, setting off a  
77 feedback cycle of performance decay that leaves it stuck in its own tracks (Mazouchova et al.,  
78 2013; McInroe et al., 2016; Schiebel et al., in review, 2019).

79 *Why study limbless locomotion in dry granular media?*

80 Despite the challenges associated with the physics of granular environments, many  
81 species move on or within these substrates. These include legged (Li et al., 2012; Qian et al.,  
82 2015), flippered (Mazouchova et al., 2013; McInroe et al., 2016) and functionally limbless  
83 species (Maladen et al., 2009; Sharpe et al., 2014; Marvi et al., 2014; Astley et al., 2015). In this  
84 Review we focus on situations in which experimentation, theory and computation have been  
85 integrated to analyze a particular form of locomotion: the use of waves of body undulation to  
86 propel the animal on and within dry granular media. Numerous terrestrial vertebrates have  
87 elongate, limbless (or functionally limbless) body plans, with most examples from squamate  
88 reptiles (Gans, 1975). Functional limblessness has evolved multiple times (Wiens et al., 2006), in  
89 deserts and other environments, and is associated with diverse locomotor behaviors (Gray, 1946;  
90 Gray and Lissmann, 1950; Jayne, 1986). For example, lateral undulation (‘slithering’) and  
91 sidewinding ([gaits we will focus on in this Review](#)) both employ posteriorly propagating waves  
92 of lateral bending, and sidewinding adds an additional vertical wave of lifting/lowering; lateral  
93 undulation and sidewinding are mostly used to move through cluttered substrates or  
94 environments dominated by open, granular substrates, respectively (Gray, 1946; Gray and  
95 Lissmann, 1950; Jayne, 1986). These behaviors are dominated by frictional forces, with minimal  
96 inertial effects (Hu et al., 2009).

97  
98 Surprisingly, limbless locomotion on granular media provides opportunities to gain  
99 insights into these substrates and terrestrial locomotion more broadly; a combination of factors  
100 creates a tractable system for examining fundamental concepts in locomotion, such as  
101 neuromechanical phase lags, control “templates” (Full and Koditschek, 1999) and morphological  
102 and behavioral adaptations. First, dry granular substrates can pose substantial challenges to such  
103 locomotors, and thus may drive behavioral or morphological adaptations (Marvi et al., 2014;  
104 Tingle et al., 2017). However unlike more complex terrestrial environments, the granular natural  
105 habitat is often homogeneous and obstacles are sparse, making these environments particularly  
106 amenable to creation of laboratory model systems. Tools (Fig 1A) allowing repeatable and  
107 standardized preparation of granular media into ecologically relevant initial conditions are  
108 relatively straightforward to develop (in contrast, studies of wet soils and muds often rely on  
109 substrate mimics (Dorgan et al., 2005)). The rheology (see Glossary) of granular media makes  
110 certain locomotion situations relatively straightforward to analyze, and subsurface locomotion is

111 governed by relatively simple forces whose forms are similar to early theoretical approaches  
112 taken to understand movement in fluids at low Reynolds numbers (e.g. spermatozoa, nematode  
113 worms (Hatton et al., 2013; Goldman, 2014)); wet substrate systems display richer but often  
114 more complicated interactions (Hosoi and Goldman, 2015; Dorgan, 2015; Sharpe et al., 2015;  
115 McKee et al., 2016). Because environmental forces dominate inertial ones in dry granular  
116 systems (like in the world of microscopic organisms), purely kinematic models can capture the  
117 motion of animals (Purcell, 1977; Gong et al., 2015; Rieser et al., in review). Furthermore,  
118 simple mathematical models ('resistive force theory') can capture a wide range of granular  
119 preparations, from particles of different size, roughness, compaction and incline (Li et al., 2013;  
120 Marvi et al., 2014); such models can also apply more broadly to frictional (but non-flowing)  
121 interactions (Rieser et al., in review ).

## 122 **Understanding locomotion through dry granular media: tools and techniques**

123 We now describe the suite of experimental, computational and theoretical tools we have  
124 developed to gain insight into granular locomotion, and which can be applied more broadly to  
125 other terrestrial locomotion scenarios.

### 126 *Experimental tools*

127 Recent progress in the study of locomotion in granular media has furnished a variety of  
128 tools that allow us to investigate and quantify the movements of limbless animals on and within  
129 granular media with remarkable thoroughness (Fig. 1). The fluidized bed is one of the most  
130 crucial tools – an apparatus that solves the problems of both regional heterogeneities in sand  
131 properties and history-dependence (e.g. retention of tracks and disturbed media) by allowing the  
132 entire sand bed to be reset to a standard state for each experimental trial (Fig. 1A) (Li et al.,  
133 2009; Qian et al., 2015). In a fluidized bed, air is propelled by an air blower through a metallic  
134 honeycomb supporting a porous plastic surface that is impermeable to granular particles and  
135 upon which the medium rests (Fig. 1A). This airflow fluidizes the **granular medium**, removing  
136 any prior disturbances and irregularities. Upon cessation of the airflow, the medium falls into a  
137 standardized state (Li et al., 2009). Further modifications to enhance the utility of fluidized beds  
138 are available, including shaker motors and air pulses to control the packing fraction of the  
139 granular media (Li et al., 2009) and sub-fluidization airflow to reduce yield force (Brzinski &  
140 Durian, 2010; Gravish et al., 2010; Zhang et al., 2013). Movement on granular media can be  
141 tracked using standard and high-speed videography and motion-capture technology (although  
142 observing foot kinematics can be a challenge (Li et al., 2012); subsurface motion can be tracked  
143 using cineradiography (Maladen et al., 2009; Ding et al., 2013; Sharpe et al., 2013; Sharpe et al.,  
144 2014) (Fig. 1A).

145 Finally, physical modeling using robots (i.e. 'robophysics'), provides a powerful tool to  
146 explore the interactions between locomotors and the granular substrate (Aguilar et al., 2016)  
147 (Fig. 1E). The robophysics approach uses robots to discover principles of locomotion, often

148 through exploration of parameter combinations not observed in animals, thereby determining the  
149 consequences of alternative morphologies and kinematic strategies. The repeatability enabled by  
150 robots allows more consistent testing and larger sample sizes than with animals, and, when  
151 combined with fluidized beds, offers the potential for automated experiments (Qian and  
152 Goldman, 2015). Motors with appropriate feedback capabilities can measure force and position  
153 data, as well as electrical power consumption, and can provide indirect proxies for measurements  
154 that can be difficult to collect from animals (e.g. tendon force-buckles, sonomicrometry,  
155 respirometry). Lastly, robots allow validation of the mathematical tools described below  
156 (Maladen et al., 2011).

157 *Computational and Theoretical tools*

158 Small systems of granular media can be modeled by computers via “discrete-element  
159 modeling” (Ding et al., 2012; Maladen et al., 2011) (Fig. 1B), in which every particle’s  
160 interactions with other particles and with intruders (i.e. objects moving through the medium) are  
161 simulated. Although this approach is accurate, it is also computationally intensive even for  
162 systems of millions of particles; real sand beds can contain many orders of magnitude more  
163 grains. The ability to understand locomotion in the context of granular media has been  
164 substantially increased via the mathematical tool of resistive force theory (RFT) (Box  
165 1)(Maladen et al., 2009; Maladen et al., 2011; Li et al., 2013), originally developed to estimate  
166 the forces on low-Re swimmers in Stokes’ flow (Gray & Hancock, 1955) (Fig. 1C,D). RFT  
167 assumes that the total force acting on an object, like an animal’s body, is a linear, independent  
168 summation of the forces acting on its constituent parts (Box 1). The granular drag forces acting  
169 on body segments are measured in systematic experiments using intruding objects of various  
170 sizes, shapes and orientations moving though granular media in fluidized beds (Box 1). RFT  
171 calculations using these empirical measurements capture crucial aspects of movement through  
172 dry granular media, especially if history-dependent effects (e.g. footprints) are minimal and  
173 intruders move at moderate to slow speeds (Box 1) (Marvi et al., 2011; Mazouchova et al., 2013;  
174 Aguilar et al., 2016; McInroe et al., 2016).

175 Recent work has revealed that granular RFT emerges from features of PDEs known as  
176 ‘frictional plasticity models’ (Askari and Kamrin, 2016). Until recently, we have not had such  
177 equations; thus, this can be considered a major advance with great potential for future analyses.  
178 Solving the plasticity PDEs is computationally intensive; however, because RFT is accurate and  
179 straightforward, we can apply this method to calculate forces for infinitesimally small segments  
180 of a moving body (Li et al., 2013), and subsequently predict the performance of hypothetical  
181 waveforms (Maladen et al., 2009; Maladen et al., 2011) as well as power (Ding et al., 2012) and  
182 joint torques (Ding et al., 2012; Sharpe et al., 2013) (Fig. 1C,D). Thus, as in the robophysical  
183 studies, the use of RFT in modeling allows the exploration of movement patterns beyond those  
184 observed in animals. Likewise, we can test whether the animals are indeed moving optimally,  
185 and determine the consequences of alternative movement patterns (Fig. 1C,D). Further,  
186 combining RFT with analytic tools from geometric mechanics (Hatton et al., 2013) enables

187 visualization of optimal or alternative gaits and limb-coordination patterns, subject to kinematic  
188 constraints and body morphology, without the need for detailed calculations (Fig. 1F).

189 Our comparative approach uses the mechanical properties of sand, the diversity of  
190 morphology and behavior of squamate reptiles, and mathematical tools such as RFT and  
191 geometric mechanics to describe and test the functional principles of locomotion. This robust  
192 approach can test basic principles of locomotor performance, with clear applications to  
193 evolutionary biology, biomechanics and, ultimately, to robotics. Furthermore, our approach  
194 allows bi-directional transfer of knowledge between biology and physics/robotics: testing of  
195 observed and quantified biomechanical performance by animals can lead to physical insights,  
196 which in turn can allow exploration of parameter ranges beyond those observed in biology,  
197 thereby allowing direct comparison between observed behaviors and hypothetical alternatives.  
198 This reciprocal approach informs robotic potential and allows for systematic testing of biological  
199 systems, which facilitates objective tests of adaptation and optimization, and even allows us to  
200 understand the influences of phylogeny with respect to locomotor opportunity or constraint.

201

## 202 **Insights gained from sand specialists**

203 In order to demonstrate the potential insights to be gained from the study of locomotion  
204 in granular media, below we discuss recent work focused on three species that specialize in  
205 movement on or through sand: the sandfish skink (*Scincus scincus*), the Mohave shovelnose  
206 snake (*Chionactis occipitalis*) and the sidewinder rattlesnake (*Crotalus cerastes*) (Fig. 2A–C).  
207 These animals are ‘sand specialists’, because they not only inhabit dune fields, but have  
208 developed specialized modes of locomotion: sand swimming in *S. scincus* and *Ch. occipitalis*,  
209 and sidewinding in *Cr. cerastes*. These case studies will illustrate how application of the tools  
210 and methods for granular systems can provide insights into physiology, behavior, control and  
211 evolution.

### 212 *Sand swimming*

213 The sandfish (*S. scincus*) (Fig. 2A) is a quadrupedal skink, native to North Africa and the  
214 Arabian Peninsula; it takes its name from a remarkable escape behavior of rapidly diving head-  
215 first into the sand and then submerging (Arnold, 1995). Although the sandfish possesses  
216 prominent limbs, these adduct completely during sub-surface burial, resulting in functionally  
217 limbless undulatory propulsion (Maladen et al., 2009). Cineradiography of subsurface  
218 locomotion in a fluidized bed reveals that sandfish achieve rapid subsurface locomotion (~1.2  
219 body lengths/second, up to 4 Hz), but the body segments show significant rearward slipping due  
220 to media yielding around the body (Maladen et al., 2009). **To facilitate analysis, body posture**  
221 **was characterized** using number of waves on the body ( $\xi$ ) and relative body curvature ( $\kappa_m \lambda_s$ , the  
222 arclength of one wave divided by the maximum radius of curvature; Sharpe et al., 2015), a non-  
223 dimensional metric for the degree of bending, which is independent of both animal size and

number of body waves. Performance is described using metrics such as estimated center-of-mass velocity, wave efficiency and slip angle (Maladen et al., 2009; Sharpe et al., 2014). Wave efficiency ( $\eta$  - forward body speed divided by wave propagation speed) or undulation efficiency ( $\eta_u$ , forward distance moved per cycle divided by the arc length of one wave) quantify how effectively body motion is converted to forwards motion, with no slip resulting in a value of  $\eta = 1$  and no forward motion a value of  $\eta = 0$  (Maladen et al., 2009, Sharpe et al., 2015). Slip angle ( $\beta_s$ ) is defined as the angle between the vector tangent to the body axis at a given point and the velocity vector of that same point (Fig. 1C); if there is no slip, each point follows the path of the points before it and  $\beta_s$  will be zero, whereas any slipping will produce higher values. Unlike  $\eta$ ,  $\beta_s$  can be calculated within a cycle and along the body, allowing analysis of where the slip occurs along the body and in which phase of the cycle, though it can also be averaged to generate a whole-animal measurement (Sharpe et al., 2014).

Slip in sand-swimming causes a decrement to locomotor performance, raising the question of whether such slip is unavoidable, and, if so, whether the sandfish are using the waveform with the maximum undulatory efficiency ( $\eta_u$ ) possible for them. Sandfish use only a limited range of waveforms during sand-swimming (Maladen et al., 2009), so exploration of alternative kinematic strategies requires a combination of mathematical and robotic modeling. Applying RFT to simulated sandfish waveforms allows calculation of  $\eta_u$  across a range of body configurations, including some not observed in the animals, showing that the sandfish operates near the optimum waveform for its morphology in terms of  $\eta$  (Maladen et al., 2009),  $\eta_u$ ,  $\beta_s$  (Sharpe et al., 2014) and mechanical cost of transport (mCoT; Sharpe et al., 2014; Fig.3A–C). These calculations were tested using a robotic model, and the results closely matched the robot-specific RFT results (Maladen et al., 2011), as well as results of discrete element modeling (Ding et al., 2012; Maladen et al., 2011). Results from the robotic model also supported the fundamental relationship seen in the calculations involving sandfish. Torque calculated using RFT for different segments within the body closely matches observed electromyographic signals from burrowing sandfish (Sharpe et al., 2013) (Fig. 3D). This provides a potential explanation for the generalized phenomenon of neuromechanical phase lag (the temporal delay observed between muscle activity and the resultant axial bending in undulatory aquatic locomotion across many species) (Ding et al., 2013).

The efficacy and efficiency of limbless locomotion in granular systems, both on the surface and beneath, raises the question of why sandfish retain their prominent legs. During the burial phase of sand-swimming, sandfish fold their legs back against the body much like a swimming crocodile (Maladen et al., 2009). Yet, limb reduction and loss is common among scincid lizards (Wiens et al 2006; Whiting et al 2003), highlighting an apparently exceptional limbed morphology in the sandfish. To examine this, the motion of the sandfish limbs was tracked prior to, during and after burial, and the effect of limb restraint on burial speed was investigated (Sharpe, 2013). Sandfish use all four limbs to propel themselves on the surface and to plunge their snout into the substrate, but each limb pair folds back against the body as soon as

263 it is submerged (Fig. 4A-C) (Sharpe, 2013). Temporarily restraining the limbs in various  
264 combinations revealed the crucial role of the limbs (particularly the forelimbs) in sand burial  
265 (Supplemental Fig. 1D-F) (Sharpe, 2013). Thus, the limbs are used on the surface, and appear to  
266 be crucial for crossing the surface–substrate boundary.

267 The Mohave shovelnose snake (*Ch. occipitalis*) independently evolved sand-swimming  
268 behavior, and **so allows for a comparison with the sandfish to test the generality of these**  
269 **principles**. Its drastically different morphology allows further exploration into the mechanics of  
270 subsurface locomotion in sand (Sharpe et al., 2015). *Ch. occipitalis* outperforms sandfish on  
271 every metric ( $\beta_s$ ,  $\eta$  and mCoT) except speed, with burrowing speed 1/10<sup>th</sup> that of the sandfish  
272 (Sharpe et al., 2014) (Fig. 3A–C). RFT modeling shows that the improvement in snake  
273 performance is due to both lower friction between the scales and the sand and the more elongate,  
274 flexible body form, which enables the snake to access combinations of relative body curvature  
275 and number of body waves that are anatomically inaccessible to the sandfish (Sharpe et al.,  
276 2014) (Fig. 3A–C). However, both species perform close to the optimal kinematics for their body  
277 form (Sharpe et al., 2014) (Fig. 3A–C), potentially due to strong evolutionary selective pressure  
278 to minimize the tremendous mechanical demands of sand-swimming. This is an insight only  
279 possible through the combined use of living animals, cineradiography, fluidized beds, RFT and  
280 robotics in a granular system.

281 *Sidewinding*

282 Limbless vertebrates moving on the surface of granular media use all known methods of  
283 limbless vertebrate locomotion (rectilinear, concertina, lateral undulation and sidewinding; Sup.  
284 Table S1), but here we focus on sidewinding. Sidewinding illustrates a crucial aspect of  
285 movement on the surface of granular media: the ability to control the forces (and minimize  
286 yielding) on body segments by lifting and lowering portions of the body (Jayne, 1986; Marvi et  
287 al., 2014).

288 Sidewinding involves undulation in both the lateral plane (typical of snakes) *and* in the  
289 vertical plane (Fig. 2C; Fig. 5A,B). It is known in a few species of viperid snakes moving across  
290 dry sand (Mosauer, 1932; Brain, 1960; Jayne, 1986; Gans and Kim, 1992), and is also used by  
291 homalopsid and natricine snake species to traverse wet granular media (Jayne, 1986). Unlike  
292 concertina and lateral undulation, which make sliding contact with the ground that may cause  
293 yielding of granular substrates, sidewinding snakes maintain approximately (low slip) static  
294 contact points with the sand (and rigid substrates), lifting and lowering the body segments as  
295 they move (Fig. 2C; Fig. 5A,B) (Rieser et al., *in rev*).

296 The net motion of the snake that emerges from these lifting and lowering patterns  
297 resembles that of a flattened ‘helical spring’ (Mosauer, 1930) or ‘virtual tread’ (Hatton and  
298 Choset, 2010; Gong et al., 2012) rolling across the ground. This rolling motion can be  
299 decomposed into two orthogonal body waves, vertical and horizontal,  $\pm \pi/2$  ( $\pm 90^\circ$ ) out of phase

300 with each other, resulting in posteriorly propagating waves of lowered static contact and lifted  
301 movement, such that a point along the body is cyclically lifted clear of the sand, moved forward,  
302 then placed back into static contact (Fig. 2C; Fig. 5A,B) (Marvi et al., 2014; Astley et al., 2015).  
303 This two-wave template not only allows easier understanding of a visually confusing locomotor  
304 mode (Pope, 1955), but also the modeling of sidewinding in snake robots with vertical and  
305 horizontal degrees of freedom, either by application of the neuromechanical template (see  
306 Glossary; Marvi et al., 2014; Astley et al., 2015) or by two-wave-based mathematical analyses of  
307 motion-capture data to gain insight into template modulation to produce complex behaviors  
308 (Gong et al., 2015) (Fig. 5B).

309 Control of contacts with the substrate is essential to sidewinding, both in generating the  
310 fundamental locomotor template and in the modifications of this template to allow effective  
311 locomotion under different conditions. Lifting allows some body segments to interact with the  
312 substrate while others do not, a trait also used in lateral undulation (Hu et al., 2009), albeit less  
313 dramatically. In the absence of the vertical wave in the template, sidewinding simply is lateral  
314 undulation (Astley et al., 2015) – the plesiomorphic locomotor behavior in squamates, legged or  
315 non-legged. This vertical component of the template allows for subtle control, such as the ability  
316 to control the relative length of the body segments that are in contact with the granular media,  
317 which is crucial in order to ascend inclined sand with minimal slip in spite of the decreasing  
318 granular yield forces of the sand with increased incline (Fig. 5D (Marvi et al., 2014). This  
319 strategy has been replicated in a robotic model to enable successful climbing of granular slopes,  
320 and the robophysics approach has been used to test combinations of contact length and incline  
321 not observed in the snakes, thus determining the consequences of parameters not observed in  
322 nature (Fig. 5F) (Marvi et al., 2014). These robophysical tests revealed that snakes are near the  
323 optimum of a range of effective kinematics; this range decreases with increasing incline (Fig. 5F  
324 (Marvi et al., 2014).

325 Sidewinding allows snakes to overcome the challenges of surface locomotion on granular  
326 media over a wide range of conditions (Marvi et al., 2014; Astley et al., 2015); however, clear,  
327 cyclic sidewinding is known only from a handful of caenophidian species (Brain, 1960; Gans  
328 and Mendelsohn, 1972; Jayne, 1986), mostly vipers (Gans and Mendelsohn, 1972), with the  
329 additional description of a similar, but non-cyclical behavior in a Green anaconda (*Eunectes*  
330 *murinus*; Ryerson and Horwitz, 2014). The taxonomic distribution of these species across  
331 multiple clades of alethinophidian snakes raises the possibility that either sidewinding has  
332 convergently evolved multiple times or, more parsimoniously, that virtually all snakes can  
333 sidewind, to some extent, if presented with suitably challenging granular substrates.

334 To test these alternatives, we encouraged 30 snake species from a range of taxonomic  
335 groups and habitats in the Zoo Atlanta collection (Sup. Table S1) to move on our fluidized bed at  
336 0°, 10°, 20° and 27° inclines, the last being the avalanche angle of the sand. Only two of 30  
337 species used sidewinding in any condition (*Cr. cerastes* and the Northern watersnake, *Nerodia*  
338 *sipedon*, the latter only very briefly), whereas the remaining species never performed

339 sidewinding even when failing to move using other modes (Sup. Table S1, Sup. Video 1; Marvi  
340 et al., 2014). Instead, most species used either lateral undulation or concertina locomotion,  
341 sometimes resorting to the latter when the former failed, and none were capable of moving uphill  
342 at the avalanche angle like the sidewinder. Although strictly proving the absence of a behavioral  
343 trait is impossible, it is unlikely that failing animals would refuse to use an effective alternative  
344 locomotor mode if it was available to them. This suggests that sidewinding is not present in most  
345 snakes and therefore evolved independently several times.

346 The strongest predictor of performance on sand was taxonomy, specifically whether the  
347 snake was a viper – 25% of vipers we tested failed to move even on level sand, whereas all non-  
348 vipers succeeded in doing so, and only two vipers could ascend granular inclines (*Cr. cerastes*  
349 and the Speckled rattlesnake, *C. mitchellii*, the latter relying on a mix of rectilinear and  
350 concertina locomotion; Sup. Table). Although the mechanistic explanation for this discrepancy  
351 remains unknown (and is the subject of ongoing investigation), it suggests that the prevalence of  
352 sidewinding in vipers is not due to some inherent advantage of vipers (Gans and Mendelsohn,  
353 1972), but rather a fundamental locomotor deficit that prevents vipers from accessing sandy  
354 habitats without the evolution of sidewinding. This matches observations of viperid species  
355 distributions across the Mojave Desert, where several viper species inhabit consolidated terra  
356 firma substrates or rocky slopes, but regional sand dune systems are exclusively populated by  
357 sidewinders (JRM, per obs).

358 Among the snakes using lateral undulation on the granular media, some individuals did  
359 not make any progress (e.g. Fig. 5A,D), some experienced high slip but made effective forward  
360 progress (Fig. 5E,G), whereas others, including the desert-specialist *Ch. occipitalis*, moved with  
361 little slipping (Fig. 5B,C,F,H,I). Effectiveness was related to how the animal's motion remodeled  
362 the granular substrate – the tracks. Snakes that failed pushed material lateral to the long axis of  
363 the body (Fig. 5A) while successful snakes pushed material both laterally and posteriorly (Fig.  
364 5B,C).

365 Modeling lateral undulation on the surface is complicated by this material hysteresis.  
366 However, RFT accurately captured the performance of snakes which did not slip enough to re-  
367 encounter their own tracks and predicted trends giving insight into anatomic and kinematic  
368 features impacting performance. As in subsurface sand swimming, RFT predicted performance  
369 depended on body elongation (Fig. 5J, black curve, L/w-total body length divided by the width  
370 at the widest part, Fig. 5K, inset) and kinematics (Fig. 5K, black curve). In accord with this  
371 prediction, long, slender snakes moved with low slip (Fig. 5J, blue and green markers), with one  
372 exception (a viper, *Bothriechis schlegelii*), while slip was high among stout snakes. Some stout  
373 snakes were still able to progress (e.g. Fig. 5E), although slip was variable (Fig. 5J, gray  
374 markers), whereas others failed to move, undulating in place as in Fig. 5A (Fig. 5J, red markers).  
375 Among stout snakes, those using high relative curvature waveforms moved with lower slip than  
376 those at lower relative curvature (Fig. 5K), a trend captured by RFT (Fig. 5K, black curve). RFT  
377 predicted performance of those snakes which succeeded (Fig. 6J, black squares), but

378 underpredicted slip of snakes which failed (Fig. 5J, red squares). This was because the model did  
379 not include material remodeling; high-slip snakes re-encountered previously disturbed material,  
380 thus experiencing forces dependent on the changed substrate state. .

### 381 **A unifying framework for locomotion: geometric mechanics**

382        Although RFT can calculate the consequences of a particular waveform, exploration of  
383 alternative behaviors is time consuming and non-intuitive. However, by combining RFT with  
384 geometric mechanics, we can understand the performance consequences of a wide range of  
385 parameters in an intuitive way, fostering insights into the mechanical and evolutionary  
386 consequences and tradeoffs of behavior. The minimal role of inertia in many forms of movement  
387 on or in dry granular media has also facilitated the application of a mathematical framework for  
388 locomotion (referred to as ‘self-propulsion’) developed decades ago in physics. This framework  
389 can unify our understanding of locomotion by allowing diagrammatic visualization of effective  
390 (and ineffective) patterns of body undulation and limb motion. The motion of microorganisms in  
391 fluids at low Reynolds-number (Purcell, 1977) inspired the creation of a systematic approach to  
392 link ‘self-deformations’ (changes in body shape and limb position) to translations and rotations  
393 in the environment (Wilczek and Shapere, 1989; Murray and Sastry, 1993; Walsh and Sastry,  
394 1995; Ostrowski and Burdick, 1998; Melli et al., 2006; Shammas et al., 2007; Morgansen et al.,  
395 2007; Avron and Raz, 2008; Hatton and Choset, 2011; Hatton and Choset, 2013; Hatton and  
396 Choset, 2015). Although this geometric framework was originally developed for low Reynolds-  
397 number swimmers, robotic models showed it could be applied in granular media (Hatton et al.,  
398 2013), where the highly damped ‘frictional fluid’ aspects of the granular interaction result in  
399 motion that depends largely on sequences of shape changes (thus the term ‘geometric’  
400 mechanics).

401        The essential approach of geometric mechanics is to analyze the effects of transit around  
402 closed (cyclic) paths in a ‘shape space’. Such a space contains representations of all possible  
403 shapes (postures) of the organism (see examples in Fig. 6A–C) and short segments in a path in  
404 the space connect different instantaneous shapes via “self-deformations”. Broadly speaking, if  
405 we determine the coupling between small self-deformations and real world displacements, we  
406 can calculate the net movement over a cycle by summing the small displacements. This sounds  
407 simple, but solving the inverse problem of which cycles best combine the available  
408 displacements is computationally expensive and can be difficult to visualize. In recent years,  
409 advances have solved some of these difficulties (Hatton and Choset, 2015). Although initially  
410 limited to simple shapes with few joints, recent developments have allowed generalization to  
411 undulating, continuous swimmers in granular media (Hatton and Choset, 2011; Gong et al.,  
412 2016; Ramasamy and Hatton 2016; Ramasamy and Hatton 2017; Rieser et al., in prep.), by  
413 representing these body shapes as a combination of two waves whose curvature varies  
414 sinusoidally in position along the body (called serpenoid waves; Umetani and Hirose, 1975). A  
415 geometric mechanics MATLAB software package is available at <https://github.com/OSU-LRAM/GeometricSystemPlotter/releases> (Remaley 2018).

417 For systems with two shape parameters (e.g. two joint angles, or the amplitude of two  
418 modes of continuous bending), the results from the geometric mechanics approach can be  
419 visualized as a set of scalar ‘constraint curvature functions’ (which we will refer to as CCF; see  
420 Glossary) over the shape parameter space (with one CCF for each direction of translation or  
421 rotation); Fig. 6A and B show forward displacement CCFs for the sandfish and shovelnose snake,  
422 respectively. The beauty of the approach is that, given a path in the height–function space (again,  
423 a pattern of cyclic self-deformation), we can immediately determine if this is a ‘good’ or ‘bad’  
424 gait (in terms of displacement) simply by summing the amount of positive and negative surface  
425 enclosed (red and black colors in Fig. 6A–C). Given that the CCFs are generated from the  
426 environmental interactions and body morphologies, these tools therefore allow evaluation of the  
427 observed behavior of an animal and determine whether the animal is optimizing for a given  
428 performance metric (Nishikawa et al., 2007; Marvi et al., 2014; Astley et al., 2015; McInroe et  
429 al., 2016), as well as predicting the consequences of alternative morphologies and behaviors that  
430 are not observed in the animals.

431 Geometric mechanics analysis can also be used for locomotion on the surface of the sand,  
432 including locomotion with discontinuous contacts, as in the case of sidewinder rattlesnakes.  
433 Mapping the contact region onto the posture shape space (Fig. 6D), allows calculation of a CCF  
434 for sidewinding (Fig. 6E). These calculations can be repeated for animals moving on rigid  
435 surfaces with both high and low friction and compared to previously collected kinematic data  
436 (Schiebel et al., in rev.); this shows that animals use 1.5 waves per body length. **Track angle can**  
437 **be calculated from body waveform**, allowing comparison with many more species (Rieser et al.,  
438 in rev.) (Fig. 6F inset). Observed data and geometric mechanics calculations agree well,  
439 showing that snakes perform better on rigid surfaces (possibly analogous to hard-packed sand in  
440 portions of their habitat), but perform close to optimally under both conditions (Fig. 6).

441 Thus, we can return to the performance data for the species discussed above (e.g. Fig. 3)  
442 with a new ‘geometric’ eye on the problem. If we make the approximation that the animals use  
443 travelling body waves of sinusoidal local curvature, this leads to circular paths in the CCF  
444 composed of two modes that approximate the animals’ shape changes (though the actual path of  
445 the animal may be non-circular). Remarkably, the animals operate near paths that (out of all  
446 circular paths) achieve most displacement per undulation cycle (Fig. 6C), those that essentially  
447 follow zero-contours (white regions in Fig. 6A,B); thus, we can conclude that these traveling  
448 wave patterns enable the observed rapid movement within and on granular material.

449 The great power of the geometric diagrams is to provide insights into the functional  
450 consequences of an animal’s choice of a particular path through space, and potentially to  
451 understand why an animal does or does not choose a particular path. **That is, geometric**  
452 **mechanics provides candidate control templates and facilitates understanding how these**  
453 **can/should change as a function of environment, morphology, body properties, etc.** For example,  
454 because muscular contractions have a limited peak power and because speed is the product of the  
455 displacement per cycle and the cycle rate, further study is needed to determine how muscle

456 physiology, morphology and interactions with the surrounding media influence the effort  
457 required for different cycle geometries. The results of these studies will allow us to geometrically  
458 identify speed-optimal gaits that balance displacement-per-cycle against cost-per-cycle  
459 (Ramasamy and Hatton, 2016). Interestingly, these tools also work for the sand swimmers and  
460 the sidewinders, indicating applicability to both fluid-like and solid-like situations. Future  
461 research directions should thus include overlaying models of muscle dynamics onto the  
462 geometric locomotion framework, as well as collecting new *in vivo* data to test whether snakes  
463 may in fact be using a non-uniform wave amplitude (which would be an oblong path in Fig. 6B)  
464 to better take advantage of the geometry of the CCF.

465 **Conclusions and challenges**

466 These examples have shown how the study of locomotion on granular media can give  
467 substantial insights into the fundamentals of limbless locomotion, including such concepts as  
468 neuromechanical phase lags, control templates and morphological and behavioral evolution  
469 (Ding et al., 2013; Sharpe et al., 2013; Sharpe et al., 2014; Marvi et al., 2014; Astley et al.,  
470 2015). Counterintuitively, the homogenous and speed-independent, yet mechanically complex  
471 and demanding nature of these substrates makes mathematical analysis and robotic modelling  
472 more feasible than for systems such as fluids, while still imposing sufficient demands on  
473 locomotion to prompt interesting and ecologically relevant tests of evolutionary adaptations in  
474 nature. Furthermore, the triad of biology, physics and robotics applied in a coordinated manner  
475 allows the exploration of alternative morphologies and behaviors that are not testable in nature,  
476 in order to determine whether the animals are truly optimizing performance and the  
477 consequences of alternative character states. Each of these tools has strengths and weaknesses,  
478 but when used in combination, each can overcome the limitations of the other, allowing for  
479 insights that are both deeper and more broadly applicable across species. This approach thus  
480 enables the construction of hypothetical mechanical analogs to fitness landscapes, **quantifying**  
481 **the performance consequences of both observed behaviors and hypothetical alternatives in order**  
482 **to visualize tradeoffs and both local and global optima**. Considering the advances enabled by this  
483 method, we suggest that granular systems and sand-dwelling animals can function as a ‘model  
484 system’, much like model taxa, to enable deeper understanding of locomotor behavior and  
485 control in challenging environments.

486 To fully realize the potential of such systems, we must address several challenges in this  
487 area. First and foremost are the consequences of disturbance of the media by the animal itself,  
488 leaving tracks with which it may interact during subsequent locomotor cycles (Mazouchova et  
489 al., 2013; Schiebel et al., in rev.), or disturbances from other animals or forces in nature.  
490 Although such disturbances are readily observable and are certainly the norm in nature, our  
491 ability to model these disturbances is in its infancy (Mazouchova et al., 2013; Schiebel et al., in  
492 rev.). Recent work indicates the existence of a predictive model for the impact of material  
493 remodeling on the granular reaction forces and thus locomotor performance (Schiebel et al., in  
494 rev.). Such a model could be incorporated into a granular-state-dependent RFT that would

495 elucidate how organisms can mitigate deleterious effects of material disturbances or even take  
496 advantage of remodeling to further improve performance (Schiebel et al., in rev.).

497 Second, the robotic and mathematical models discussed are ‘open loop’ in design,  
498 without sensory feedback or behavioral modulation based on the environment. Although this  
499 simplification is useful for understanding robust behaviors that maintain performance without  
500 feedback, a deeper understanding of animal locomotion must incorporate the feedback and  
501 control mechanisms present in real animals. Our approach has been useful to discover control  
502 templates (Full and Koditschek, 1999), and we posit that the granular media systems will  
503 facilitate the discovery of anchors – models that describe how animal physiology and  
504 morphology integrate to produce the template behavior. As this field develops, we look forward  
505 to solutions to both of these shortcomings, with the commensurate increased understanding of  
506 these fascinating systems. Principles discovered in this tractable, yet complex locomotor  
507 substrate may provide insights into more complex substrates, such as heterogeneous and  
508 cohesive granular media (Winter et al., 2014; Qian and Goldman, 2015; Dorgan, 2015).

509 **Acknowledgements**

510 This research was supported by National Science Foundation (NSF) Grants 1150760,  
511 ECCS-0846750, CMMI 1653220 and 0848894; NSF funding for the Student Research Network  
512 in the Physics of Living Systems Grant 1205878; Army Research Office Grant  
513 W911NF1010343; the Army Research Laboratory under Cooperative Agreement No. W911NF-  
514 10-2-0016; the Georgia Institute of Technology School of Biology and Elizabeth Smithgall Watts  
515 endowment; DIG thanks the Dunn Family Professorship. The views and conclusions contained  
516 in this document are those of the authors and should not be interpreted as representing the  
517 official policies, either expressed or implied, of the Army Research Laboratory or the US  
518 Government. The US Government is authorized to reproduce and distribute reprints for  
519 Government purposes notwithstanding any copyright notation herein.

520 **Glossary**

521 **Constraint curvature function (CCF)** – Diagrams which enable visualization and rapid  
522 calculation of performance for different cyclic patterns of “self-deformation” (like lateral  
523 undulation wave shapes).

524 Coulomb friction – A model for friction between dry surfaces, in which the frictional force is  
525 proportional to the normal force between the surfaces and independent of surface area or speed.

526 Fluidization – The process of forcing a fluid flow through a granular media, which will then  
527 behave as a fluid until the flow drops below a minimum speed.

528 Frictional fluid – When flowing, granular media behaves as a frictional fluid with some  
529 similarities to low Reynolds number (Re) flows. **In low Re flow, the viscous forces overwhelm**

530 inertia effects, while in frictional fluids, the frictional forces between particles overwhelm  
531 inertial effects. This facilitates the use of mathematical tools and concepts from analysis of low  
532  $Re$  locomotion to be applied to granular media.

533 Granular media – A substrate composed of many particles in contact with each other. These  
534 particles may interact via friction or, in wet systems, capillary adhesion.

535 Jamming – A phenomenon in which the friction between particles of granular media reaches  
536 equilibrium with the applied force, causing deformation of the media to cease.

537 Neuromechanical template – A simplified model describing the fundamental dynamics and  
538 motion of an animal during locomotion, which serves as a target for control; the spring-loaded  
539 inverted pendulum (SLIP) model of walking is a neuromechanical template.

540 Packing fraction – The fraction of a volume occupied by granular particles. Granular media in a  
541 close-packed state will have many particles in a given volume and many inter-particle contacts,  
542 whereas a loose-packed state will have fewer particles and contacts. Small changes in packing  
543 fraction can have large consequences for values such as yield stress.

544 Rheology – The study of flowing matter, including fluids, plastically deforming solids and  
545 granular media

546 Yield stress – The force per unit area necessary to overcome frictional forces in the granular  
547 media and cause yielding deformation.

548

549 Box 1 – Resistive force theory

550 If we imagine an animal as being made of many small segments, the motion of a body segment  
551 through the surroundings can be described by its orientation and velocity – i.e. some angle,  $\psi$ ,  
552 between the segment's tangent and velocity vectors. Using granular drag experiments, we can  
553 empirically determine an equation relating the motion of an object to the resulting granular  
554 stress. One drags an intruder (for example a cylinder model for a body segment or a flat plate  
555 representing a section of body wall) through the granular media of interest and measures the  
556 forces on the intruder as it moves through the media. One can then average the force in the  
557 steady state to obtain an estimate of the granular reaction force acting on a body part during  
558 steady-state locomotion. By carrying out these measurements over a range of  $\psi$ , one builds a  
559 continuous function relating segment motion to force using a range of curve-fitting methods (e.g.  
560 Fourier fit, polynomial fit, splines).

561 The tangent of a segment is determined by the shape and self-deformation of the animal. The  
562 velocity of the segment has two contributors; there is a velocity associated with the change of  
563 shape from one time point to the next, and there is a velocity arising from movement of the  
564 animal's center of mass (CoM). The former is determined solely by the self-deformation,  
565 whereas the latter arises from the interaction of the animal with the environment. Given the  
566 dissipative nature of granular media, we assume that the force on each body segment can be  
567 calculated independently of all other segments, such that the total force on the animal is simply  
568 the sum of these individual contributions. The force on a segment is related to  $\psi$  by the empirical  
569 equation. The angle  $\psi$  changes with the CoM velocity, so, for the prescribed kinematics, the RFT  
570 calculation numerically searches for the CoM velocity that yields zero net force on the body.

571

572 **References**

573 **Agarwal, S., Karsai, A., Goldman, D.I., and Kamrin, K.** in prep. A generalized resistive force  
574 theory for rate-dependent intrusion phenomena in granular media, in prep.

575 **Aguilar, J., Zhang, T., Qian, F., Kingsbury, M., McInroe, B., Mazouchova, N., Li, C.,**  
576 **Maladen, R. D., Gong, C., Travers, M., et al.** (2016). A review on locomotion  
577 robophysics: the study of movement at the intersection of robotics, soft matter and  
578 dynamical systems. *Reports Prog. Phys.* **79**, 110001.

579 **Andreotti, B., Forterre, Y. and Pouliquen, O.** (2013). *Granular Media: Between Fluid and*  
580 *Solid*. Cambridge: Cambridge University Press.

581 **Arnold, E. N.** (1995). Identifying the effects of history on adaptation: origins of different sand-  
582 diving techniques in lizards. *J. Zool. London* **235**, 351–388.

583 **Askari, H. and Kamrin, K.** (2016). Intrusion rheology in grains and other flowable materials.  
584 *Nat. Mater.* **15**, 1274–1279.

585 **Astley, H. C.** Traversing Tight Tunnels—Implementing an Adaptive Concertina Gait in a  
586 Biomimetic Snake Robot. in Earth and Space 2018, 16th Biennial International Conference  
587 on Engineering, Science, Construction, and Operations in Challenging Environments 158–  
588 168 (American Society of Civil Engineers, 2018). doi:10.1061/9780784481899.017

589 **Astley, H. C., Gong, C., Dai, J., Travers, M., Serrano, M. M., Vela, P. A., Choset, H.,**  
590 **Mendelson, J. R., Hu, D. L. and Goldman, D. I.** (2015). Modulation of orthogonal body  
591 waves enables high maneuverability in sidewinding locomotion. *Proc. Natl. Acad. Sci. U. S.*  
592 *A.* **112**,

593 **Avron, J. E. and Raz, O.** (2008). A geometric theory of swimming: Purcell’s swimmer and its  
594 symmetrized cousin. *New J. Phys.* **10**, 063016.

595 **Baum, M. J., Heepe, L. and Gorb, S. N.** (2014). Friction behavior of a microstructured  
596 polymer surface inspired by snake skin. *Beilstein J. Nanotechnol.* **5**, 83–97.

597 **Brain, C. K.** (1960). Observations on the locomotion of the south west African adder, *Bitis*  
598 *peringueyi* (Boulenger), with speculations on the origin of sidewinding. *Ann. Transvaal*  
599 *Museum* **24**, 19–24.

600 **Brzinski, T. A. and Durian, D. J.** (2010). Characterization of the drag force in an air-moderated  
601 granular bed. *Soft Matter* **6**, 3038–3043.

602 **Cohen, K. E., Hernandez, L. P., Crawford, C. H. and Flammang, B. E.** (2018). Channeling  
603 vorticity: modeling the filter-feeding mechanism in silver carp using  $\mu$ CT and 3D PIV. *J.*  
604 *Exp. Biol.* **221**, jeb.183350.

605 **Collins, S., Ruina, A., Tedrake, R. and Wisse, M.** (2005). Efficient bipedal robots based on  
606 passive-dynamic walkers. *Science* **307**, 1082–5.

607 **Coulomb C.A., (1776).** Essai sur une application des regles des maximis et minimis a quelques

608        problemes de statique relatifs a l'architecture. *Memoires de l'Academie Royale pres Divers*  
609        *Savants*, 7

610        **Ding, Y., Sharpe, S. S., Masse, A. and Goldman, D. I.** (2012). Mechanics of Undulatory  
611        Swimming in a Frictional Fluid. *PLoS Comput Biol* **8**, e1002810.

612        **Ding, Y., Sharpe, S. S., Wiesenfeld, K. and Goldman, D. I.** (2013). Emergence of the  
613        advancing neuromechanical phase in a resistive force dominated medium. *Proc. Natl. Acad.*  
614        *Sci. U. S. A.* **110**, 9746–9751.

615        **Dorgan, K. M.** (2015). The biomechanics of burrowing and boring. *J. Exp. Biol.* **218**, 176–83.

616        **Dorgan, K. M., Jumars, P. A., Johnson, B., Boudreau, B. P. and Landis, E.** (2005). Burrow  
617        extension by crack propagation. *Nature* **433**, 475–475.

618        **Full, R. J. and Koditschek, D. E.** (1999). Templates and anchors: neuromechanical hypotheses  
619        of legged locomotion on land. *J. Exp. Biol.* **202**, 3325–3332.

620        **Gans, C.** (1975). Tetrapod limblessness: evolution and functional corollaries. *Am. Zool.* **15**, 455–  
621        467.

622        **Gans, C. and Kim, H.** (1992). Kinematic description of the sidewinding locomotion of four  
623        vipers. *Isr. J. Zool.* **38**, 9–23.

624        **Gans, C. and Mendelsohn, H.** (1972). Sidewinding and jumping progression in vipers. In  
625        *Proceedings of the 2nd International Symposium, Toxins of Animal and Plant Origin* (ed. de  
626        Vries, A.) and Kochva, E.), pp. 17–38. London: Gordon and Breach Science Publishers.

627        **Gemmell, B. J., Fogerson, S. M., Costello, J. H., Morgan, J. R., Dabiri, J. O. and Colin, S.**  
628        **P.** (2016). How the bending kinematics of swimming lampreys build negative pressure  
629        fields for suction thrust. *J. Exp. Biol.* **219**, 3884–3895.

630        **Geng, J. and Behringer, R. P.** (2005). Slow drag in two-dimensional granular media. *Phys.*  
631        *Rev. E* **71**, 11302.

632        **Goldman, D. I.** (2014). Colloquium : Biophysical principles of undulatory self-propulsion in  
633        granular media. *Rev. Mod. Phys.* **86**, 943–958.

634        **Gong, C., Hatton, R. L. and Choset, H.** (2012). Conical sidewinding. In *2012 IEEE*  
635        *International Conference on Robotics and Automation*, pp. 4222–4227. IEEE.

636        **Gong, C., Travers, M. J., Astley, H. C., Li, L., Mendelson, J. R., Goldman, D. I. and Choset,**  
637        **H.** (2015). Kinematic gait synthesis for snake robots. *Int. J. Rob. Res.*

638        **Gong, C., Goldman, D. I. and Choset, H.** (2016). Simplifying Gait Design via Shape Basis  
639        Optimization. *Robot. Sci. Syst.* **12**,

640        **Gravish, N., Umbanhowar, P. B. & Goldman, D. I.** (2010) Force and Flow Transition in  
641        Plowed Granular Media. *Phys. Rev. Lett.* **105**, 128301.

642        **Gray, J.** (1946). The mechanism of locomotion in snakes. *J. Exp. Biol.* **23**, 101–120.

643 **Gray, J. and Hancock, G. J.** (1955). The Propulsion of Sea-Urchin Spermatozoa. *J. Exp. Biol.*  
644 32, 802-814.

645 **Gray, J. and Lissmann, H. W.** (1950). The kinetics of locomotion of the grass snake. *J. Exp.*  
646 *Biol.* **94**, 15–42.

647 **Hatton, R. L. and Choset, H.** (2010). Sidewinding on slopes. In *2010 IEEE International*  
648 *Conference on Robotics and Automation*, pp. 691–696. IEEE.

649 **Hatton, R. and Choset, H.** (2011). Kinematic Cartography for Locomotion at Low Reynolds  
650 Numbers. *Proc. Robot. Sci. Syst. VII* 1–8.

651 **Hatton, R. L. and Choset, H.** (2013). Geometric Swimming at Low and High Reynolds  
652 Numbers. *IEEE Trans. Robot.* **29**, 615–624.

653 **Hatton, R. L. and Choset, H.** (2015). Nonconservativity and noncommutativity in locomotion.  
654 *Eur. Phys. J. Spec. Top.* **224**, 3141–3174.

655 **Hatton, R. L., Ding, Y., Choset, H. and Goldman, D. I.** (2013). Geometric Visualization of  
656 Self-Propulsion in a Complex Medium. *Phys. Rev. Lett.* **110**, 78101.

657 **Holmes, P., Full, R. J., Koditschek, D. and Guckenheimer, J.** (2006). The Dynamics of  
658 Legged Locomotion: Models, Analyses, and Challenges. *SIAM Rev.* **48**, 207–304.

659 **Hosoi, A. E. and Goldman, D. I.** (2015). Beneath Our Feet: Strategies for Locomotion in  
660 Granular Media. *Annu. Rev. Fluid Mech.* **47**, 431–453.

661 **Hu, D. L., Nirody, J., Scott, T. and Shelley, M. J.** (2009). The mechanics of slithering  
662 locomotion. *Proc. Natl. Acad. Sci.* **106**, 10081–10085.

663 **Jayne, B. C.** (1986). Kinematics of terrestrial snake locomotion. *Copeia* **1986**, 195–208.

664 **Lauder, G. V.** (2010). Swimming hydrodynamics: ten questions and the technical approaches  
665 needed to resolve them. In *Animal Locomotion*, pp. 3–15. Berlin, Heidelberg: Springer  
666 Berlin Heidelberg.

667 **Li, C., Umbanhowar, P. B., Komsuoglu, H., Koditschek, D. E. and Goldman, D. I.** (2009).  
668 Sensitive dependence of the motion of a legged robot on granular media. *Proc. Natl. Acad.*  
669 *Sci.* **106**, 3029–3034.

670 **Li, C., Hsieh, S. T. and Goldman, D. I.** (2012). Multi-functional foot use during running in the  
671 zebra-tailed lizard (*Callisaurus draconoides*). *J. Exp. Biol.* **215**, 3293–3308.

672 **Li, C., Zhang, T. and Goldman, D. I.** (2013). A Terradynamics of Legged Locomotion on  
673 Granular Media. *Science (80-. ).* **339**, 1408–1412.

674 **Lissmann, H. W.** Rectilinear Locomotion in a Snake (*Boa Occidentalis*). *J. Exp. Biol.* **26**, 368–  
675 379 (1950).

676 **Maladen, R. D., Ding, Y., Li, C. and Goldman, D. I.** (2009). Undulatory swimming in sand:  
677 subsurface locomotion of the sandfish lizard. *Science* **325**, 314–8.

678 **Maladen, R. D., Ding, Y., Umbanhowar, P. B. and Goldman, D. I.** (2011). Undulatory  
679 swimming in sand: experimental and simulation studies of a robotic sandfish. *Int. J. Rob.  
680 Res.* **30**, 793–805.

681 **Maladen, R. D., Ding, Y., Umbanhowar, P. B., Kamor, A. and Goldman, D. I.** (2011).  
682 Mechanical models of sandfish locomotion reveal principles of high performance  
683 subsurface sand-swimming. *J. R. Soc. Interface* **8**, 1332–1345.

684 **Marvi, H. and Hu, D. L.** (2012). Friction enhancement in concertina locomotion of snakes. *J. R.  
685 Soc. Interface* **9**, 3067–3080.

686 **Marvi, H., Bridges, J. and Hu, D. L.** (2013). Snakes mimic earthworms: Propulsion using  
687 rectilinear travelling waves. *J. R. Soc. Interface* **10**, 20130188.

688 **Marvi, H., Meyers, G., Russell, G. and Hu, D. L.** (2011). Scalybot: A Snake-Inspired Robot  
689 With Active Control of Friction. In *ASME 2011 Dynamic Systems and Control Conference  
690 and Bath/ASME Symposium on Fluid Power and Motion Control, Volume 2*, pp. 443–450.  
691 ASME.

692 **Marvi, H., Gong, C., Gravish, N., Astley, H., Travers, M., Hatton, R. L., Mendelson, J. R.,  
693 Choset, H., Hu, D. L. and Goldman, D. I.** (2014). Sidewinding with minimal slip: snake  
694 and robot ascent of sandy slopes. *Science* **346**, 224–9.

695 **Mazouchova, N., Gravish, N., Savu, A. and Goldman, D. I.** (2010). Utilization of granular  
696 solidification during terrestrial locomotion of hatchling sea turtles. *Biol. Lett.* **6**, 398–401.

697 **Mazouchova, N., Umbanhowar, P. B. and Goldman, D. I.** (2013). Flipper driven terrestrial  
698 locomotion of a sea turtle inspired robot. *Bioinspirations & Biomimetics* **8**, 26007.

699 **McInroe, B., Astley, H. C., Gong, C., Kawano, S. M., Schiebel, P. E., Rieser, J. M., Choset,  
700 H., Blob, R. W. and Goldman, D. I.** (2016). Tail use improves performance on soft  
701 substrates in models of early vertebrate land locomotors. *Science (80-. ).* **353**,.

702 **McKee, A., MacDonald, I., Farina, S. C. and Summers, A. P.** (2016). Undulation frequency  
703 affects burial performance in living and model flatfishes. *Zoology* **119**, 75–80.

704 **Melli, J. B., Rowley, C. W. and Rufat, D. S.** (2006). Motion Planning for an Articulated Body  
705 in a Perfect Planar Fluid. *SIAM J. Appl. Dyn. Syst.* **5**, 650–669.

706 **Morgansen, K. A., Triplett, B. I. and Klein, D. J.** (2007). Geometric Methods for Modeling  
707 and Control of Free-Swimming Fin-Actuated Underwater Vehicles. *IEEE Trans. Robot.* **23**,  
708 1184–1199.

709 **Mosauer, W.** (1930). A Note on the Sidewinding Locomotion of Snakes. *Am. Nat.* **64**, 179–183.

710 **Mosauer, W.** (1932). Adaptive convergence in the sand reptiles of the Sahara and of California:  
711 a study in structure and behavior. *Copeia* **1932**, 72–78.

712 **Murray, R. M. and Sastry, S. S.** (1993). Nonholonomic motion planning: steering using  
713 sinusoids. *IEEE Trans. Automat. Contr.* **38**, 700–716.

714 **Newman, S. J. and Jayne, B. C.** Crawling without wiggling: muscular mechanisms and  
715 kinematics of rectilinear locomotion in boa constrictors. *J. Exp. Biol.* **221**, jeb.166199  
716 (2018).

717 **Nishikawa, K., Biewener, A. A., Aerts, P., Ahn, A. N., Chiel, H. J., Daley, M. A., Daniel, T.**  
718 **L., Full, R. J., Hale, M. E., Hedrick, T. L., et al.** (2007). Neuromechanics: an integrative  
719 approach for understanding motor control. *Integr. Comp. Biol.* **47**, 16–54.

720 **Ostrowski, J. and Burdick, J.** (1998). The Geometric Mechanics of Undulatory Robotic  
721 Locomotion. *Int. J. Rob. Res.* **17**, 683–701.

722 **Pope, C. H.** (1955). *The reptile world; a natural history of the snakes, lizards, turtles, and*  
723 *crocodilians*. New York: Knopf.

724 **Purcell, E. M.** (1977). Life at low Reynolds number. *Am. J. Phys.* **45**, 3–11.

725 **Qian, F. and Goldman, D. I.** (2015). The dynamics of legged locomotion in heterogeneous  
726 terrain: universality in scattering and sensitivity to initial conditions. In *Robotics: Science*  
727 *and Systems*, p. Rome, Italy.

728 **Qian, F., Zhang, T., Korff, W., Umbanhowar, P. B., Full, R. J. and Goldman, D. I.** (2015).  
729 Principles of appendage design in robots and animals determining terradynamic  
730 performance on flowable ground. *Bioinspir. Biomim.* **10**, 56014.

731 **Ramasamy, S. and Hatton, R. L.** (2016). Soap-bubble optimization of gaits. In *2016 IEEE 55th*  
732 *Conference on Decision and Control (CDC)*, pp. 1056–1062.

733 **Ramasamy, S. & Hatton, R. L.** (2017) Geometric gait optimization beyond two dimensions. In  
734 *2017 American Control Conference (ACC)*, pp. 642–648. doi:10.23919/ACC.2017.7963025

735 **Rieser, J. M., Gong, C., Astley, H. C., Schiebel, P. E., Hatton, R. L., Choset, H. and**  
736 **Goldman, D. I.** *in review*. Geometric phase and dimensionality reduction in locomoting  
737 living systems.

738 **Remaley, J. L.** (2018). Improving Understanding of Geometric Swimmer Locomotion. Oregon  
739 State University.  
740 [https://ir.library.oregonstate.edu/concern/graduate\\_thesis\\_or\\_dissertations/m900p088t](https://ir.library.oregonstate.edu/concern/graduate_thesis_or_dissertations/m900p088t)

741 **Ryerson, W. G. and Horwitz, S.** (2014). *Eunectes murinus* (Green Anaconda),  
742 Behavior/Sidewinding. *Herpetol. Rev.* **45**, 337–338.

743 **Savage, S. B.** (1984). The Mechanics of Rapid Granular Flows. *Adv. Appl. Mech.* **24**, 289–366.

744 **Schiebel, P. E., Astley, H. C., Rieser, J. M., Agarwal, S., Hubicki, C., Hubbard, A. M.,**  
745 **Cruz, K., Mendelson, J., Kamrin, K. and Goldman, D. I.** (2019). Mitigating memory  
746 effects during undulatory locomotion on hysteretic materials. *bioRxiv* 748186.

747 **Purcell, E. M.** (1977). Life at low Reynolds number. *Am. J. Phys.* **45**, 3–11.

748 **Schofield, A. N. and Wroth, P.** (1968). *Critical state soil mechanics*. McGraw-Hill.

749 **Shammas, E. A., Choset, H. and Rizzi, A. A.** (2007). Geometric Motion Planning Analysis for  
750 Two Classes of Underactuated Mechanical Systems. *Int. J. Rob. Res.* **26**, 1043–1073.

751 **Sharpe, S. S.** (2013). Control of burial and subsurface locomotion in particulate substrates. PhD.  
752 Thesis, Georgia Institute of Technology.

753 **Sharpe, S. S., Ding, Y. and Goldman, D. I.** (2013). Environmental interaction influences  
754 muscle activation strategy during sand-swimming in the sandfish lizard *Scincus scincus*. *J.  
755 Exp. Biol.* **216**, 260–274.

756 **Sharpe, S. S., Koehler, S. A., Kuckuk, R. M., Serrano, M., Vela, P. A., Mendelson, J. and  
757 Goldman, D. I.** (2014). Locomotor benefits of being a slender and slick sand-swimmer. *J.  
758 Exp. Biol.*

759 **Sharpe, S. S., Kuckuk, R. and Goldman, D. I.** (2015). Controlled preparation of wet granular  
760 media reveals limits to lizard burial ability. *Phys. Biol.* **12**, 046009.

761 **Tingle, J. L., Gartner, G. E. A., Jayne, B. C. and Garland, T.** (2017). Ecological and  
762 phylogenetic variability in the spinalis muscle of snakes. *J. Evol. Biol.* **30**, 2031–2043.

763 **Tobalske, B. W.** (2007). Biomechanics of bird flight. *J. Exp. Biol.* **210**, 3135–3146.

764 **Tytell, E. D., Hsu, C.-Y., Williams, T. L., Cohen, A. H. and Fauci, L. J.** (2010). Interactions  
765 between internal forces, body stiffness, and fluid environment in a neuromechanical model  
766 of lamprey swimming. *Proc. Natl. Acad. Sci.* **107**, 19832–19837.

767 Umbanhowar P. B. and Goldman, D. I. (2006) Low density fragile states in cohesive powders.  
768 *American Journal of Physics*, **74**, 720-721

769 **Umetani, Y. and Hirose, S.** (1975). Biomechanical Study on Serpentine Locomotion. *Trans.  
770 Soc. Instrum. Control Eng.* **11**, 20–24.

771 **Vogel, S.** (1994). *Life in moving fluids : the physical biology of flow*. Princeton University Press.

772 **Waldrop, L. D. and Miller, L. A.** (2015). The role of the pericardium in the valveless, tubular  
773 heart of the tunicate *Ciona savignyi*. *J. Exp. Biol.* **218**, 2753–63.

774 **Walsh, G. C. and Sastry, S. S.** (1995). On reorienting linked rigid bodies using internal  
775 motions. *IEEE Trans. Robot. Autom.* **11**, 139–146.

776 **Whiting, A. S., Bauer, A. M. and Sites, J. W.** Phylogenetic relationships and limb loss in sub-  
777 Saharan African scincine lizards (Squamata: Scincidae). *Mol. Phylogenet. Evol.* **29**, 582–  
778 598 (2003).

779 **Wiens, J. J., Brandley, M. C. and Reeder, T. W.** (2006). Why Does A Trait Evolve Multiple  
780 Times Within A Clade? Repeated Evolution Of Snakeline Body Form In Squamate  
781 Reptiles. *Evolution (N. Y.)* **60**, 123–141.

782 **Wilczek, F. and Shapere, A.** (1989). *Geometric Phases in Physics*. World Scientific.

783 **Winter, A. G., V, Deits, R. L. H., Dorsch, D. S., Slocum, A. H. and Hosoi, A. E.** (2014).  
784       Razor clam to RoboClam: burrowing drag reduction mechanisms and their robotic  
785       adaptation. *Bioinspir. Biomim.* **9**, 036009.

786 **Wise, T. N., Schwalbe, M. A. B. and Tytell, E. D.** (2018). Hydrodynamics of linear  
787       acceleration in bluegill sunfish, *Lepomis macrochirus*. *J. Exp. Biol.* **221**, jeb190892.

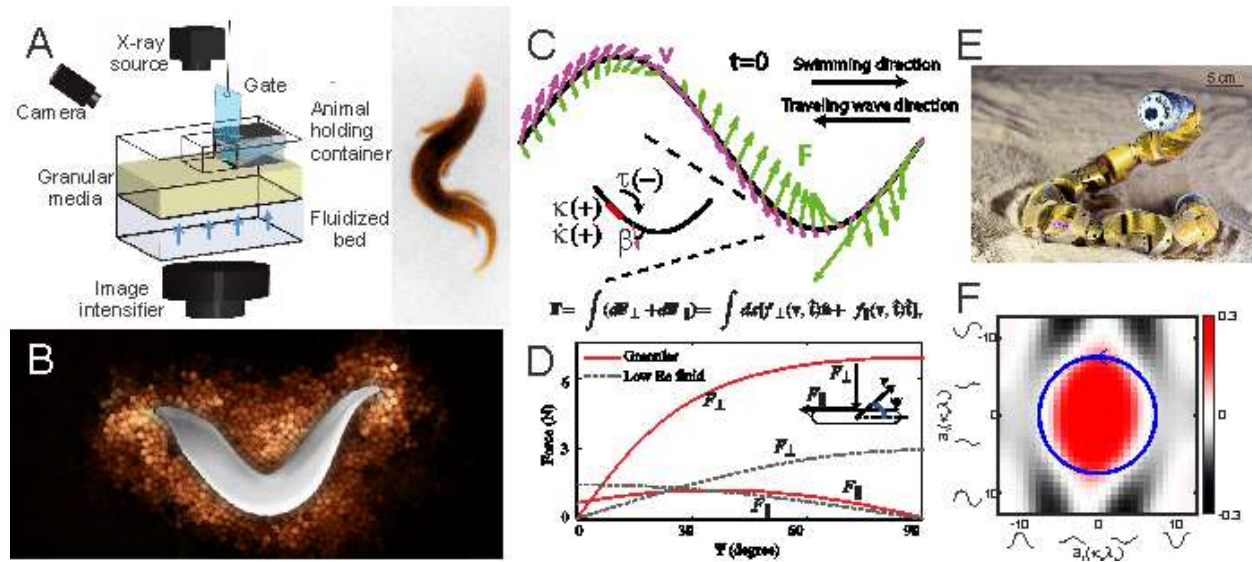
788 **Zhang, T., Qian, F., Li, C., Masarati, P., Hoover, A. M., Birkmeyer, P., Pullin, A., Fearing,  
789       R. S. and Goldman, D. I.** (2013). Ground fluidization promotes rapid running of a  
790       lightweight robot. *International Journal of Robotics Research*, pp. 859–869.

791

792

793

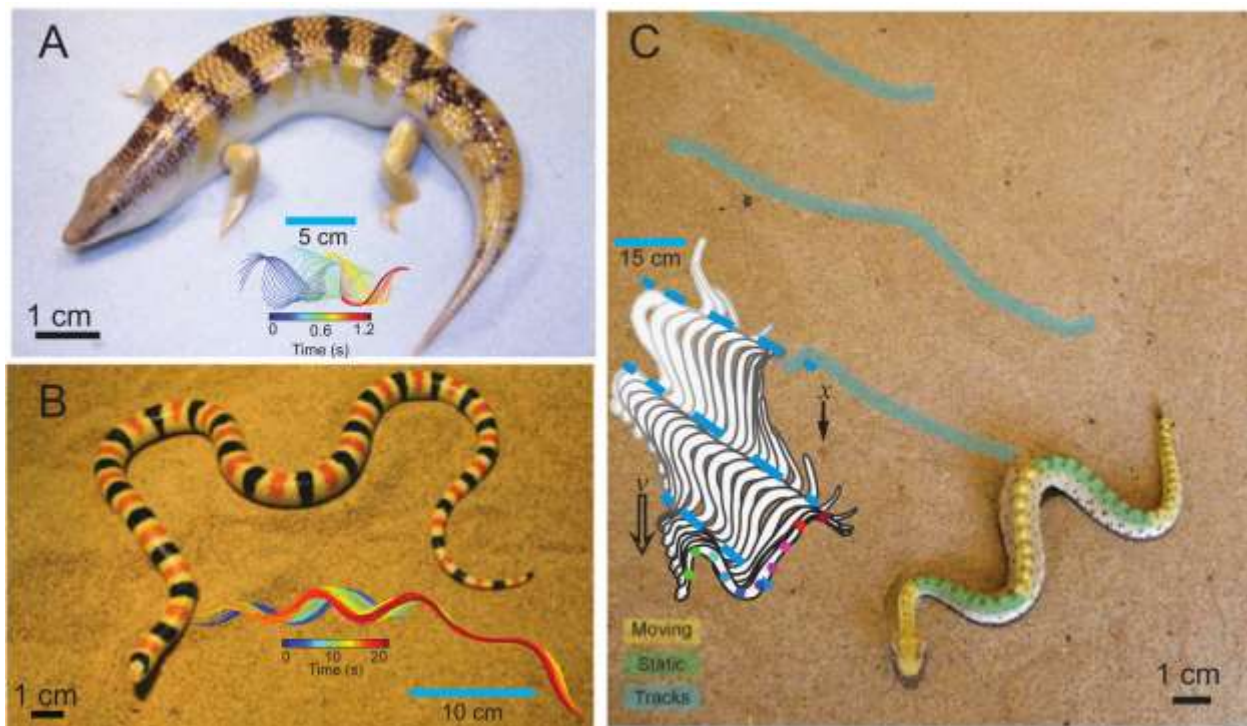
794

795 **Figures & Captions**

796

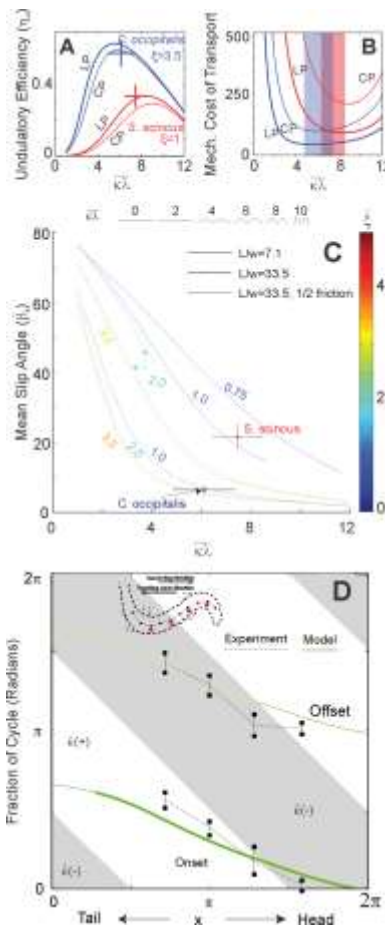
797 **Figure 1 – Tools for studying locomotion on and within granular media.** (A) A fluidized bed  
 798 filled with granular media (yellow), showing the semipermeable base and airflow (blue arrows),  
 799 situated for cineradiography (modified from Sharpe et al 2014); inset shows a false-color X-ray  
 800 image. (B) Discrete element numerical simulation of a sandfish moving through particles.  
 801 Lighter particle color indicates higher velocity. Image from Goldman lab (C) Resistive force  
 802 theory (RFT) applied to an undulating elongate body (modified from Ding et al 2013). For each  
 803 segment, purple arrows are velocity vectors,  $v$ , green arrows are force,  $F$ . Inset shows a segment  
 804 at 0.6 body length, with the signs of curvature ( $\kappa$ ), curvature change ( $\kappȧ$ ), torque ( $\tau$ ) and slip angle  
 805 ( $\beta$ ). Red region indicates the predicted side of muscle activity at a given site. (D) Perpendicular  
 806 and parallel forces ( $F_{\perp}, F_{\parallel}$ ) versus orientation angle ( $\psi$ ) of a cylinder dragged through dry  
 807 granular media and low Re fluid. Equation for force is shown at the top;  $ds$ , the length of a small  
 808 element of the curve;  $v$ , velocity;  $t$ , orientation;  $n$ , perpendicular to the orientation (modified  
 809 from Ding 2012) (E) A multi-segment robophysical model of a snake (photo from Choset lab).  
 810 (F) A constraint curvature function (CCF) from a geometric mechanics model of subsurface  
 811 movement by a sandfish skink (a limbed lizard). Waves along the axes show the relative  
 812 curvature of each body wave along the axis. Blue circle shows the path using relative body  
 813 curvature values of the animal. The color scale shows units of body lengths/ $(\kappa_m \lambda_s)^2$ , a metric of  
 814 body curvature (see text), multiplied by 100.

815



816  
817 **Figure 2 – Example species for studying locomotion on and within granular media.** (A) The  
818 sandfish skink (*Scincus scincus*). Inset shows a time sequence of subsurface movement.  
819 Modified from Sharpe et al., 2014. (B) The Mohave shovelnose snake (*Chionactis occipitalis*).  
820 Inset shows a time sequence of subsurface movement. Modified from Sharpe et al., 2014. (C)  
821 The sidewinder rattlesnake (*Crotalus cerastes*). Photo from the Astley lab. Inset shows a time  
822 sequence of movement. Modified from Marvi et al., 2014. Inset scale bars are blue, main image  
823 scale bars are black.

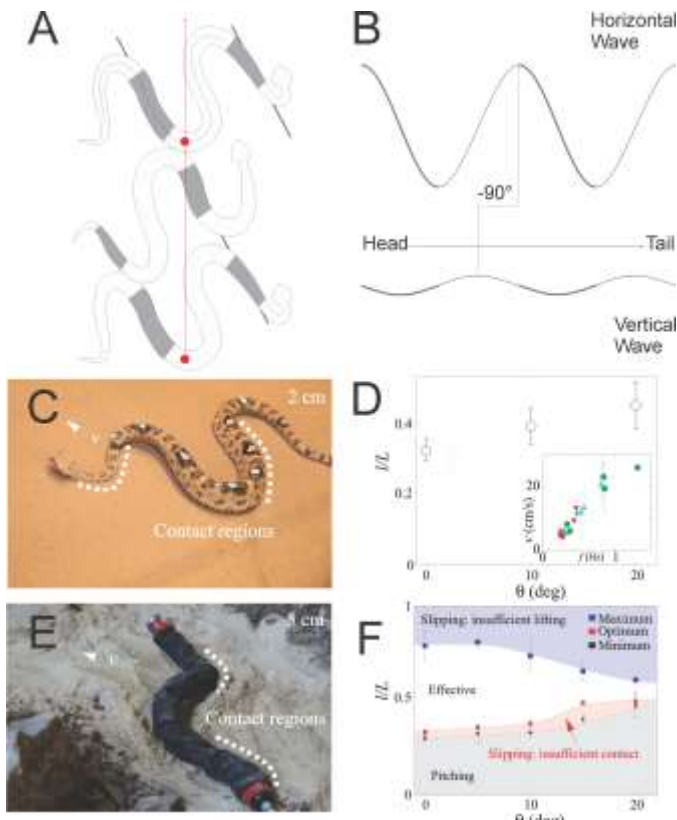
824



825

826 **Figure 3 – Comparison of experiments and models of sand-swimming in sandfish and**  
 827 **shovelnose snake.** (A) Curves depicting undulatory efficiency ( $\eta_u$ ) for RFT-calculated  
 828 undulating bodies with the skin friction and wave number ( $\xi$ ) observed in the animals (sandfish  
 829 shown in red and shovelnose snake shown in blue), at various mean relative body curvatures  
 830 ( $\kappa_m \lambda_s$ ). LP and CP denote loose-packed and close-packed sand. + symbols denote the range of  $\eta_u$   
 831 and  $\kappa_m \lambda_s$  observed in each animal. (B) Curves depicting mechanical cost of transport at various  
 832 body curvatures ( $\kappa_m \lambda_s$ ) as in A. Shaded regions denote the range of  $\kappa_m \lambda_s$  observed in each  
 833 animal. (C) Mean slip angle ( $\beta_s$ ) at various body curvatures ( $\kappa_m \lambda_s$ ), with line type denoting  
 834 different combinations of body length/width ratios ( $L/w$ ) and friction. + symbols denote the  
 835 range of  $\beta_s$  and  $\kappa_m \lambda_s$  observed in each animal. Color scale indicates wave number ( $\xi$ ). (D)  
 836 Neuro-mechanical phase lag predicted by an RFT model compared to experimental data on EMG  
 837 onset and offset. The horizontal axis shows position along the body, and the vertical axis shows  
 838 the fraction of a cycle, expressed in radians, where  $2\pi$  is a complete locomotor cycle. Increasing  
 839 body curvature  $\kappa(+)$  and decreasing body curvature  $\kappa(-)$  are indicated by white and grey regions,  
 840 respectively. Inset shows electrode implant sites (red). A–C modified from Sharpe et al., 2014;  
 841 D modified from Ding et al., 2013.

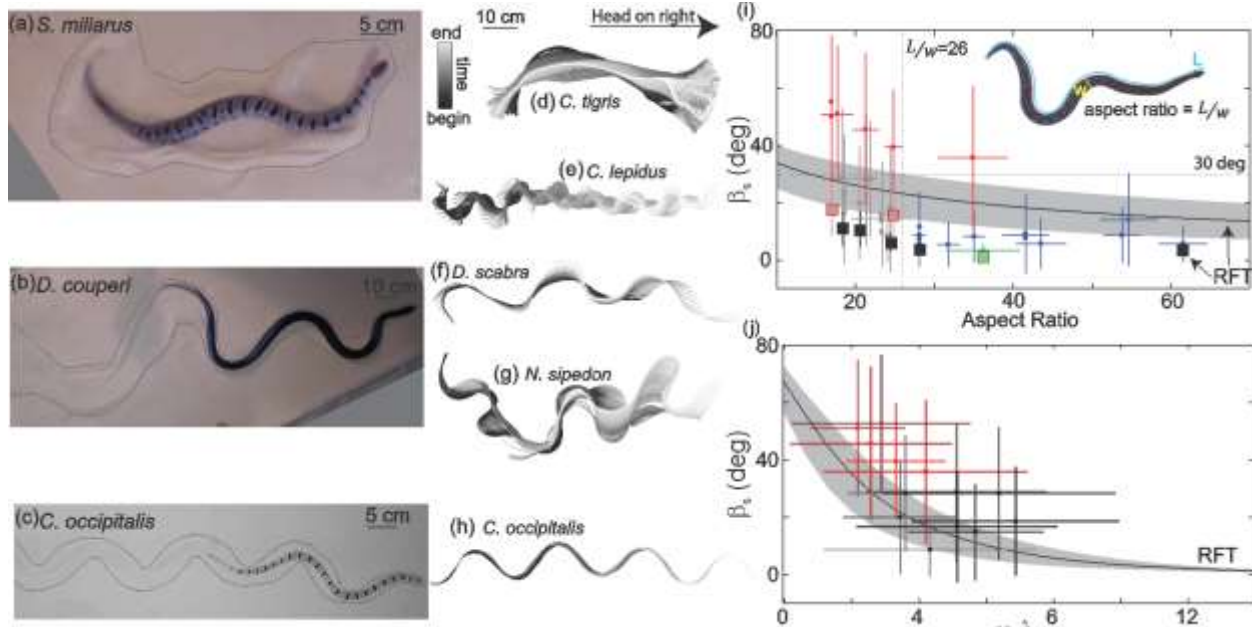
842



843

844 **Figure 4 – Sidewinding on sand.** (A) Schematic of sidewinding, showing three sequential  
 845 postures. Static regions of the body are shaded grey, as are the consequent tracks; white regions  
 846 are moving and are lifted above the substrate. Black squares indicate markers on the body, while  
 847 the red arrow shows the direction of motion for a given point (red dot) over a cycle. Modified  
 848 from Astley et al., 2015. (B) Sidewinding represented by a horizontal and vertical wave offset by  
 849  $-\pi/2$ . Grey shaded regions are in static contact with the ground. Modified from Astley et al.,  
 850 2015. (C) An example frame for a sidewinder ascending a slope, showing the direction of  
 851 movement (arrow) and contact regions (white dashed lines). (D) Change in contact length as a  
 852 fraction of total body length ( $I/L$ ) in sidewinders on slopes of 0, 10 and 20 degrees. Inset graph  
 853 shows the relationship between speed and frequency. (E) An example frame of video of a robot  
 854 snake ascending a slope by sidewinding, showing the direction of movement (arrow) and contact  
 855 regions (white dashed lines). (F) Consequences of different relative contact lengths ( $I/L$ ) for a  
 856 robot on the same range of slopes as the sidewinders. Light grey, light blue and light red regions  
 857 indicate robot failures due to pitching, slipping due to insufficient lifting, and slipping due to  
 858 insufficient contact, respectively; blue and black squares indicate observed robot data at the  
 859 maximum and minimum contact lengths resulting in forward progress; red ‘optimal’ squares  
 860 show the highest velocity contact length. The white region shows effective sidewinding by the  
 861 robot. C–F modified from Marvi et al. 2014. **Error bars in D and F are standard deviation.**

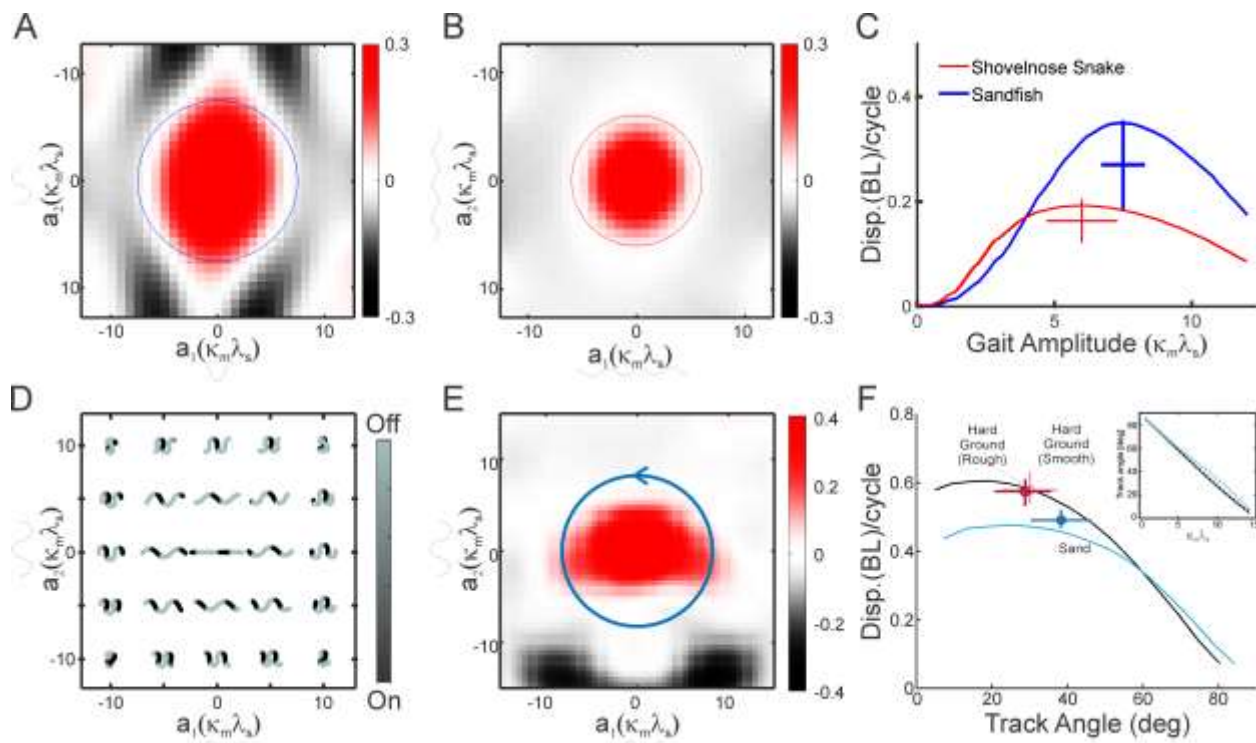
862



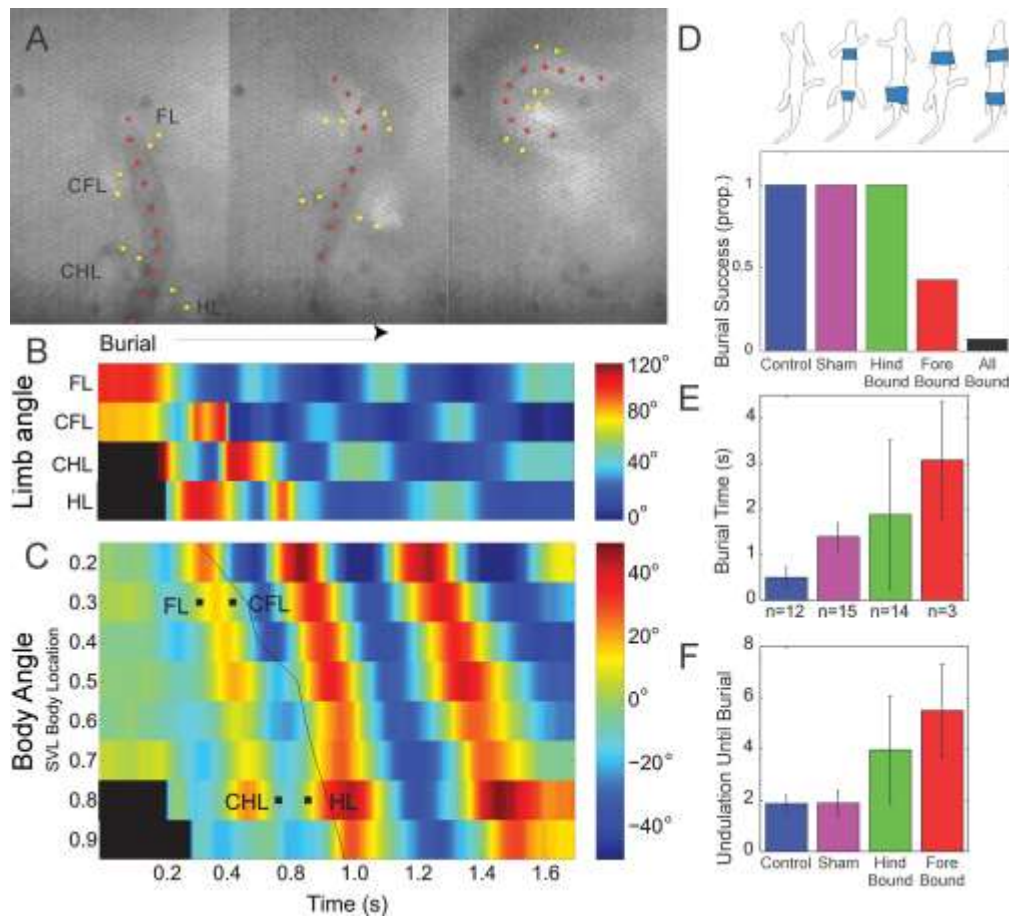
863  
864 **Figure 5 - Body shape and kinematics impact ability to progress across granular surface.**

865 (A–C) Snapshots of snakes moving on the surface of GM. Dashed lines indicate the disturbed  
866 area. (A) *Sistrurus miliarius*, on natural sand collected from Yuma, Arizona, USA. (B)  
867 *Drymarchon couperi*. Same sand as A. (C) *Ch. occipitalis* on 300  $\mu$ m glass particles. (D–I)  
868 Digitized animal midlines colored by time from beginning (dark) to end (light) of the trial. D–G  
869 are on Yuma sand; H–I are on glass particles. (D) *Crotalus tigris*, trial length ( $t_{tot}$ )=25.7 s, time  
870 between plotted midlines ( $\Delta t$ )=100 ms. (E) *Cr. lepidus*,  $t_{tot}$ =9.4 s,  $\Delta t$ =33 ms. (F) *Dasypeltis*  
871 *scabra*,  $t_{tot}$ =1.6 s,  $\Delta t$ =33 ms. (G) *Nerodia sipedon*,  $t_{tot}$ =6.0 s,  $\Delta t$ =33 ms. (H) *Ch. occipitalis*,  
872 individuals 130  $t_{tot}$ =1.25 s,  $\Delta t$ =12 ms. (I) Slip versus L/w (inset, *Acrantophis dumerili*  
873 L/w=23.2. Circle markers and vertical lines indicate the mean and standard deviation of each  
874 trial. Horizontal bars are the range of aspect ratios measured from video stills by two different  
875 researchers. Gray are successful trials, red are failures, green is *Ch. occipitalis*. Markers at the  
876 same L/w indicate multiple trials for the same individual. N=22 animals, n=38 animal trials.  
877 Only the mean is shown for *Ch. occipitalis* N=9, n=30. Black curve is the RFT prediction of slip  
878 using average snake waveform and mass and a scale friction  $\mu$ =0.15. Gray area indicates  
879 predictions for estimated min/max  $\mu$ =0.1 (lower slip) and 0.2 (higher slip). Scale friction  
880 estimated using Hu et al., 2009; Baum et al., 2014. Square markers are the RFT prediction of slip  
881 for that animal using a scale friction of  $\mu$ =0.15, vertical line is the min/max. For *Ch. occipitalis*,  
882  $\mu$ =0.1 (Sharpe et al., 2015) and min/max=0.05/0.15. All RFT predictions used force relations for  
883 300  $\mu$ m glass beads at an intrusion depth of 8 mm. (J) Slip versus  $\kappa_m \lambda_s$  for animals with L/w<26.  
884 Mean and standard deviation from combined trials of an individual are shown. Successful trials in  
885 black, failures in red, square marker is the snake with L/w>26. Black curve is the RFT prediction  
886 using average waveform and anatomy of all species studied, wave number ( $\xi$ )=2.5, mass=0.63  
887 kg, L=89 cm,  $\mu$ =0.15. Gray band is min/max  $\mu$ =0.1/0.2. (L) Success versus failure of snakes on  
888 sand at various angles. 25% of viper species failed to move on level sand, whereas all non-  
889 vipers (including pythons, boas and colubrids) succeeded, regardless of native habitat. All vipers  
890 failed on slopes except sidewinders and a speckled rattlesnake (*Cr. mitchellii*), which used a

891 combination of concertina and rectilinear locomotion to ascend extremely slowly. Non-vipers  
892 were more likely to be successful.



895 **Figure 6: Geometric mechanics of locomotion in granular media.** Constraint curvature  
 896 functions (CCFs) for the sandfish lizard (A) and shovelnose snake (B); the color scale shows  
 897 units of body lengths /  $(\kappa_m \lambda_s)^2$ , multiplied by 100. A and B show the paths for the mean relative  
 898 curvature ( $\kappa_m \lambda_s$ ) observed in the animals (solid circle), with  $a_1$  and  $a_2$  representing the amplitude  
 899 of the relative body curvature ( $\kappa_m \lambda_s$ ) for the two wave components. (C) The displacement per  
 900 cycle predicted using geometric mechanics (solid curves) and animal data for subsurface  
 901 movement; vertical and horizontal lines on animal data are  $\pm$  one standard deviation. (D) Shape  
 902 space showing a posture-dependent animal–environment contact model for an animal with 1.5  
 903 waves along its body during sidewinding. (E) CCF for sidewinding on sand with 1.5 waves along  
 904 the body. The blue circle shows the average performance of *Cr. cerastes* on sand. (F)  
 905 Comparison of geometric mechanics predictions to biological data for the movement of different  
 906 animals on different substrates. Dark red, *Cr. cerastes* on a rough rigid surface; light red, *Cr.*  
 907 *cerastes* on a smooth rigid surface; blue, *Cr. cerastes* on a 7.6-cm layer of sand. Inset: track  
 908 angle versus relative curvature along the body for sand (blue) and hard ground (black).

911 **Supplementary Figures, Tables and Videos**

912

913 **Supplementary Figure 1 – Limb use during burial in sandfish.** (A) A series of stills from an  
 914 X-ray video of a sandfish during initial burial at 240 ms intervals. Red dots indicate lead  
 915 markers on the vertebral midline, while yellow dots indicate markers on the forelimb (FL),  
 916 contralateral forelimb (CFL), hindlimb (HL) and contralateral hindlimb (CHL). (B) Limb  
 917 position during burial and subsurface locomotion. High angles denote a protracted posture, low  
 918 angles a retracted posture. Black areas were out of the field of view. (C) Body angle during  
 919 burial and subsurface locomotion. Black squares indicate the final retraction of the designated  
 920 limb, and the black line the approximate time of burial of that body segment. D-F) Experimental  
 921 manipulation of limb use, including control and sham treatments, indicated by outlines. (D)  
 922 Proportion of successful burials in each treatment. (E) Average time until complete burial for  
 923 each treatment; sample size given on the horizontal axis, all-bound state omitted due to low N.  
 924 (F) Number of body undulations until complete burial for each treatment; all-bound state omitted  
 925 due to low N.

926

927

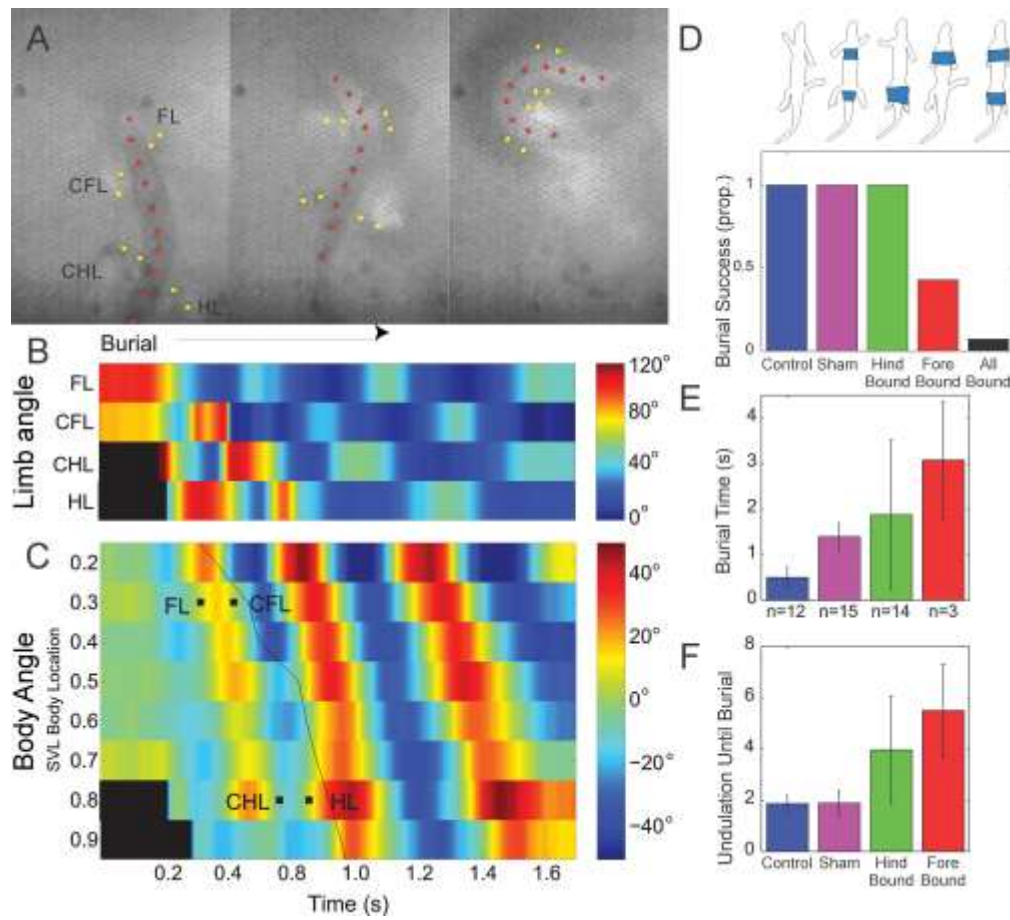
928      Supplementary Figure 1 - Limb use during burial in sandfish. A) A series of stills from an X-ray  
929      video of a sandfish during initial burial at 240 ms intervals. Red dots indicate lead markers  
930      on the vertebral midline, while yellow dots indicate markers on the forelimb (FL),  
931      contralateral forelimb (CFL), hindlimb (HL) and contralateral hindlimb (CHL). B) Limb  
932      position during burial and subsurface locomotion. High angles denote a protracted posture,  
933      low angles a retracted posture. Black areas were out of the field of view. C) Body angle  
934      during burial and subsurface locomotion. Black squares indicate the final retraction of the  
935      designated limb, and the black line the approximate time of burial of that body segment. D-  
936      F) Experimental manipulation of limb use, including control and sham treatments, indicated  
937      by outlines. D) Proportion of successful burials in each treatment. E) Average time until  
938      complete burial for each treatment; sample size given on the horizontal axis, all-bound state  
939      omitted due to low N. F) Number of body undulations until complete burial for each  
940      treatment; all-bound state omitted due to low N.

941      Supplementary Video 1 –Dorsal view videos of selected snake species moving on level and  
942      inclined sand. When inclined, uphill is to the right.

943      Supplementary Table 1 – Observed modes of locomotion of snakes on granular media at various  
944      inclines. Columns from left to right show species name, mass, total length, maximum  
945      midbody diameter, maximum incline angle of effective locomotion, and observed modes on  
946      level, 10°, 20°, and 28°, with the last being the avalanche angle of the sand. LU is lateral  
947      undulation, SW is sidewinding, Conc. is concertina, and Rect. is rectilinear. Locomotor  
948      modes followed by parenthetical (Fail) denotes failure to move on that incline and the  
949      modes used during attempted locomotion. All included species attempted to move on the  
950      listed diameters; species which did not attempt locomotion (e.g. defensive displays) were  
951      excluded from trials.

952

953 Supplementary Figure 1



954

955